JGR Biogeosciences

RESEARCH ARTICLE
10.1029/2022JG006824

Turbidity Currents Can Dictate Organic Carbon Fluxes Across River-Fed Fjords: An Example From Bute Inlet (BC, Canada)

S. Hage[1,2,3,4], V. V. Galy[5], M. J. B. Cartigny[4], C. Heerema[4,6], M. S. Heijnen[7], S. Acikalin[8], M. A. Clare[7], I. Giesbrecht[9,10], D. R. Gröcke[11], A. Hendry[8], R. G. Hilton[12], S. M. Hubbard[2], J. E. Hunt[7], D. G. Lintern[13], C. McGhee[8], D. R. Parsons[14], E. L. Pope[4], C. D. Stacey[13], E. J. Sumner[3], S. Tank[9,15], and P. J. Talling[4,11]

[1]University of Brest, CNRS, Ifremer, Geo-Ocean, Plouzané, France, [2]Department of Geoscience, University of Calgary, Calgary, AB, Canada, [3]School of Ocean and Earth Sciences, University of Southampton, Southampton, UK, [4]Department of Geography, Durham University, Durham, UK, [5]Department of Marine Chemistry and Geochemistry, Woods Hole Oceanographic Institution, Woods Hole, MA, USA, [6]Department of Geography, University of Victoria, Victoria, BC, Canada, [7]Ocean BioGeosciences, National Oceanography Centre Southampton, Southampton, UK, [8]School of Natural and Environmental Sciences, Newcastle University, Newcastle, UK, [9]Hakai Institute, Vancouver, BC, Canada, [10]School of Resource and Environmental Management, Simon Fraser University, Burnaby, BC, Canada, [11]Department of Earth Sciences, Durham University, Durham, UK, [12]Department of Earth Sciences, University of Oxford, Oxford, UK, [13]Geological Survey of Canada, Natural Resources Canada, Sidney, BC, Canada, [14]Energy and Environment Institute, University of Hull, Hull, UK, [15]Department of Biological Sciences, University of Alberta, Edmonton, AB, Canada

Abstract The delivery and burial of terrestrial particulate organic carbon (OC) in marine sediments is important to quantify, because this OC is a food resource for benthic communities, and if buried it may lower the concentrations of atmospheric CO_2 over geologic timescales. Analysis of sediment cores has previously shown that fjords are hotspots for OC burial. Fjords can contain complex networks of submarine channels formed by seafloor sediment flows, called turbidity currents. However, the burial efficiency and distribution of OC by turbidity currents in river-fed fjords had not been investigated previously. Here, we determine OC distribution and burial efficiency across a turbidity current system within Bute Inlet, a fjord in western Canada. We show that 62% ± 10% of the OC supplied by the two river sources is buried across the fjord surficial (30–200 cm) sediment. The sandy subenvironments (channel and lobe) contain 63% ± 14% of the annual terrestrial OC burial in the fjord. In contrast, the muddy subenvironments (overbank and distal basin) contain the remaining 37% ± 14%. OC in the channel, lobe, and overbank exclusively comprises terrestrial OC sourced from rivers. When normalized by the fjord's surface area, at least 3 times more terrestrial OC is buried in Bute Inlet, compared to the muddy parts of other fjords previously studied. Although the long-term (>100 years) preservation of this OC is still to be fully understood, turbidity currents in fjords appear to be efficient at storing OC supplied by rivers in their near-surface deposits.

Plain Language Summary Plants on land use CO_2 from the atmosphere to produce organic carbon, which promotes their growth. Rivers transport organic carbon to the sea, where it is either eaten by fauna or buried in the seafloor, thus decreasing atmospheric CO_2 levels on Earth over thousands to millions of years. Fjords are recognized as global organic carbon sinks; trapping 18 million tons of organic carbon in their seafloor sediments each year. However, the complex morphology of fjord seafloors was not considered in the calculation of this organic carbon flux. In this study, we determine the distribution and abundance of terrestrial organic carbon across a fjord (Bute Inlet, Canada), which contains a submarine channel network terminating onto a large accumulation of sand (called a lobe). We show that 62% of the organic carbon supplied by the two rivers connected to the fjord is buried across the fjord; the majority of this carbon being held in the lobe. In total, Bute Inlet buries at least 3 times more organic carbon per unit of surface area than other fjords previously studied. Submarine channels in fjords thus appear to promote the storage of land-derived organic carbon in the seafloor, potentially impacting CO_2 levels and food resources for marine fauna.

Key Points:

- Bute Inlet, a river-fed fjord incised by turbidity currents, has a contemporary terrestrial organic carbon burial efficiency of 62% ± 10%
- Sandy surficial deposits are responsible for 63% ± 14% of the total terrestrial organic carbon burial budget in Bute Inlet, but only cover 17% of the seafloor area
- Global estimates based only on the muddy parts of fjords may significantly underestimate organic carbon burial rates by a factor >3

Supporting Information:

Supporting Information may be found in the online version of this article.

Correspondence to:

S. Hage,
sophie.hage@univ-brest.fr

Citation:

Hage, S., Galy, V. V., Cartigny, M. J. B., Heerema, C., Heijnen, M. S., Acikalin, S., et al. (2022). Turbidity currents can dictate organic carbon fluxes across river-fed fjords: An example from Bute Inlet (BC, Canada). *Journal of Geophysical Research: Biogeosciences*, *127*, e2022JG006824. https://doi.org/10.1029/2022JG006824

Received 7 FEB 2022
Accepted 9 MAY 2022

1. Introduction

The sequestration of terrestrial particulate organic carbon (OC) in marine sediments can lead to a drawdown of atmospheric CO_2 and thus form a long-term control on carbon dioxide and oxygen levels in Earth's atmosphere (Berner, 1982; Burdige, 2007; Hilton & West, 2020). Terrestrial OC also constitutes a key energy resource

for benthic communities living on the seabed, including in fjords (Hunter et al., 2013; Włodarska-Kowalczuk et al., 2019). It is therefore important to constrain the fluxes of terrestrial OC delivered to the seabed over short (decades to centuries) and long (thousand to million year) timescales. Major river deltas worldwide bury about 47 Mt of terrestrial OC each year, approximately 30% of the total OC burial including marine organic matter in the oceans (Berner, 1989; Burdige, 2007; Hedges & Keil, 1995). Despite their surface areas being 40 times smaller than that of deltas and continental shelves, fjords have been shown to represent 17% of the global terrestrial OC burial (Cui, Bianchi, Jaeger, et al., 2016; Cui, Bianchi, Savage, et al., 2016). Therefore, fjord systems are hotspots for OC sequestration (Cui, Bianchi, Jaeger, et al., 2016; Cui, Bianchi, Savage, et al., 2016; Cui et al., 2017; Smith et al., 2015). However, these global OC burial estimates in fjords are based on samples taken predominantly from the muddy parts of fjords and assume the seafloor in fjords is homogeneous in terms of OC burial and sedimentation rates (SRs).

Fjord seafloors can, however, be highly heterogeneous (Bianchi et al., 2020; Smeaton & Austin, 2019) and comprise diverse subenvironments including submarine channels, and associated overbanks and lobes (Conway et al., 2012; Pope et al., 2019; Zeng et al., 1991). Such subenvironments are created by submarine sediment density flows, called turbidity currents. These flows distribute sediment and OC across the fjord floor, connecting river mouths to the deeper parts of fjords, and fractionate sediment and OC by grain size and density en-route. Only a handful of studies have discussed how OC is distributed and fractionated within fjords (Bianchi et al., 2020; Cui, Bianchi, Jaeger, et al., 2016; Cui, Bianchi, Savage, et al., 2016; Cui et al., 2017; Hage et al., 2020; Smeaton & Austin, 2019). For example, a recent study of Scottish fjords revealed that muddy (<63 μm) sediments held the largest amounts of OC (~2.6 Mt) compared to sandy sediment (~0.26 Mt; Smeaton & Austin, 2019). While the OC budgets are known in the Scottish fjords, the processes determining these budgets remain uncertain, partly because of a lack of bathymetric data and knowledge of submarine flow processes in these settings (e.g., these Scottish fjords may not contain active turbidity currents). In contrast, a study of Bute Inlet (a fjord in British Columbia, Canada) highlighted that the sandy parts of a submarine channel formed by turbidity currents held large amounts of OC (Hage et al., 2020). Higher OC content in sandy submarine channels compared to the nonchannelized environments was also observed in Steffen Fjord (Chile; Vanderkerkhove et al., 2020). However, the river-derived OC inputs and burial rates in different subenvironments created by turbidity currents were not considered in that previous study of Bute Inlet, nor in any other fjord. Given the large variation and uncertainty in OC burial efficiency between fjord subenvironments, it is important to assess this variability more accurately to estimate global OC budgets (Burdige, 2007; Smith et al., 2015) and to improve paleoclimate/environmental reconstructions based on sediment cores in fjords (Bianchi et al., 2020).

Here for the first time, we quantify the amount and type of OC supplied by two rivers and its distribution in the surficial sediments (top 2 m) of different subenvironments (e.g., channel floor, overbanks, lobe, and distal basin) across a river-fed fjord. This study then shows how OC is unevenly distributed within a fjord and illustrates how OC distribution and burial is dependent on turbidity current processes. Insights into how OC is distributed have wider implications for understanding OC burial by turbidity currents in locations other than fjords, for which there are also very few detailed OC budgets from river sources to marine sinks. Therefore, we compare our Bute Inlet results with available information on how OC is distributed in sandier or muddier subenvironments of other turbidity current systems, that is, Gaoping (Kao et al., 2014; Liu et al., 2016), Ganges–Brahmaputra (Galy et al., 2007; Lee et al., 2019), and Congo (Baudin et al., 2020). This comparison highlights whether similar or contrasting OC burial patterns emerge more generally.

The main objective of this paper is to constrain OC fluxes from source to sink in Bute Inlet by answering the following questions: (a) how much OC is delivered by the two rivers discharging into Bute Inlet? (b) How much and what type of OC is present in the Bute Inlet subenvironments? (c) What is the terrestrial OC burial efficiency of Bute Inlet and how does it compare with other fjords? Finally, we discuss the study in a wider global context and thus compare our results from Bute Inlet with (nonfjord) deep-sea turbidity current systems.

2. Bute Inlet: A Fjord Fed by Two Rivers

Bute Inlet is a 78-km-long fjord in British Columbia, Canada (Figure 1). The inlet has an average width of ~4 km, an average depth of 550 m (with a maximum of 660 m; Prior et al., 1987), and a total surface area of 273 km^2 (including the fjord's steep sidewalls).

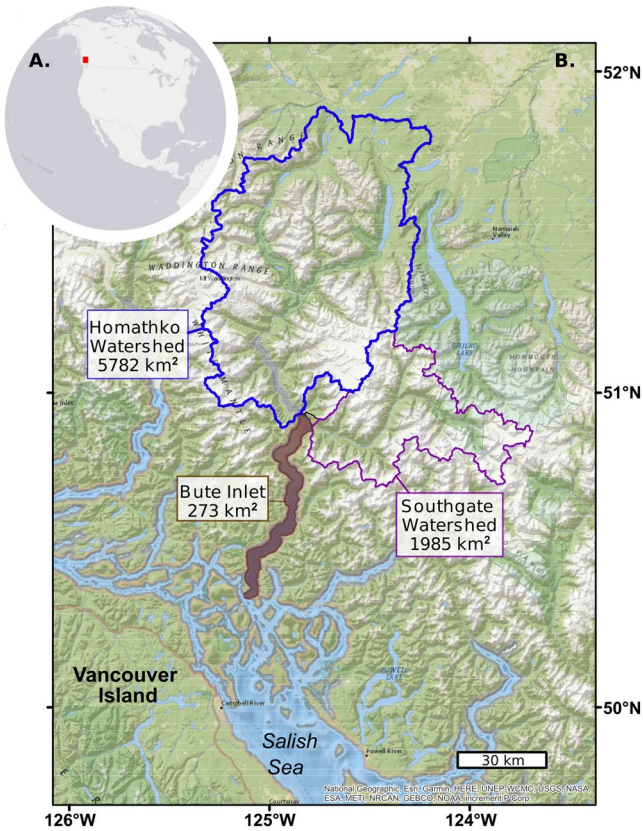

Figure 1. (a) Location of Bute Inlet in British Columbia (Canada). (b) Bute Inlet is fed by Homathko and Southgate Rivers. Watershed areas were delimited by Gonzalez Arriola et al. (2018).

2.1. Homathko and Southgate Rivers

The Homathko and Southgate Rivers feed the head of Bute Inlet (Figure 1). The watersheds of both rivers are supplied by meltwater from snow and glaciers within their catchment (e.g., Homathko has a 19.1% glacier cover, while Southgate has a 33.5% glacier cover) leading to sustained high flow in summer (Giesbrecht et al., 2022). An estimated 1,684 and 2,089 mm of mean annual precipitation (~60% as snow) occurred between 1981 and 2010 (Wang et al., 2016) in the Homathko and Southgate Rivers, respectively (Giesbrecht et al., 2022). Rainforest vegetation and soils predominate below treeline on the Pacific side of the Coast Mountains (Meidinger & Pojar, 1991). The river floodplains are populated by coniferous and deciduous forests. These two rivers provide 94% of the freshwater and sediment inputs into the fjord, with the remainder of the freshwater being provided by small streams entering the fjord at its margins (Farrow et al., 1983). The watershed areas are 5,782 and 1,985 km^2 for Homathko and Southgate Rivers, respectively (Figure 1; Gonzalez Arriola et al., 2018). The Homathko River has an average annual discharge of 250 m^3/s, with an average summer peak discharge of ~800 m^3/s (Water Survey of Canada, 2020). The average annual suspended sediment flux of the Homathko River is 30 kg/s, whereas its bedload discharge is 99 kg/s (Table 1; Syvitski & Farrow, 1983). There was no gauging station in the Southgate River up to 2021. However, recent (2021) data and the covariation between daily discharge on the two systems allowed the Southgate discharge (water and total suspended load) to be modeled for our years of interest (Table 1; Texts S1–S4 in Supporting Information S1).

During the spring and summer meltwater period (freshet), the rivers create large sediment-laden freshwater plumes at the fjord's head (Syvitski et al., 1985; Tabata & Pickard, 1957). These plumes flow on top of the denser more saline fjord water, thereby bringing terrestrial particles into the fjord and enhancing the heterotrophic activity of bacterioplankton (Albright, 1983). Due to the relatively large tidal range (up to 5.5 m), sediment from these river plumes is likely to be concentrated in a turbidity maximum that is located in between the fresh and saline water (Dyer, 1997). Observations in a similar and nearby fjord setting (Howe Sound, Canada) show that during the freshet these turbidity maxima can hold enough sediment to become denser than the saline fjord water (Hage et al., 2019). During spring tides, the river plume becomes more focused and powerful, so that low tides cause these dense turbidity maxima to migrate onto the steep delta slope, where they can trigger turbidity currents (Hage et al., 2019). These processes, together with submarine failures of the delta slopes, result in turbidity currents frequently being triggered in such river-fed and tide-influenced fjord settings (Clare et al., 2016; Hizzett et al., 2018). It is likely that similar initiating mechanisms for turbidity currents also occur in Bute Inlet (Hughes Clarke et al., 2015).

2.2. Bute Inlet Turbidity Current System

Downstream of the Homathko and Southgate Deltas lie two submarine channels, which merge into a single sinuous channel, formed by turbidity currents (Prior et al., 1986, 1987; Figures 2 and 3). The channel is incised into the seafloor to a depth of ~20 m on average. The channel floor is flanked by terraces that are particularly well developed in the first 10 km of the fjord. Further downstream (430–580 m water depth; Figure 3), the submarine channel becomes less incised and is flanked by levees that are variably developed (Prior et al., 1987). For simplicity, in this paper, we use the term "overbanks" (Figure 3) to describe both the muddy terraces and levees bounding the submarine channel floor in Bute Inlet along its entire length.

The sediment composition of the Bute Inlet turbidity current system has been described in older work, based on sediment cores (Prior et al., 1986; Zeng et al., 1991), yet the OC composition of these cores was not documented until recently. The OC stored within the submarine channel floor was shown to be composed mostly of young terrestrial woody debris buried within fine sands (Hage et al., 2020). In this study, we build on the findings of

Table 1
Homathko and Southgate Rivers Characteristics and Estimates of Annual Organic Carbon Fluxes

	Homathko	Southgate
Watershed area (km^2)	5,782	1,985
Glacier coverage (%)[a,b]	19.1	33.5
Contribution to Bute Inlet (%)[b]	75	19
Yearly mean discharge (m^3/s)[b]	254	141
Suspended load discharge (Kt/year)[d]	946	221
Bedload discharge (Kt/year)	4,164[c,d]	
Average TOC in river suspended load (%)	0.87 ± 0.3	
Average TOC in river bedload (%)	0.3 ± 0.2	
OC flux in river suspended load (Kt OC/year)	10.1 ± 3.3	
OC flux in river bedload (Kt OC/year)	12.6 ± 9.6	
Total riverine OC flux (Kt OC/year)	22.7 ± 13.1	

[a]Giesbrecht et al. (2022). [b]Syvitski and Farrow (1983). [c]See Text S1 in Supporting Information S1 for suspended load estimates in both rivers. [d]No bedload estimate was found in the literature for the Southgate River. The bedload was thus estimated based on the Homathko River using the ratio between the two river watersheds as a scaling factor (Text S2 in Supporting Information S1). TOC data in river samples are included in Figure 5 and Table S7 in Supporting Information S1.

Hage et al. (2020) from the channel floor, by documenting the distribution of OC across all of the subenvironments within this turbidity current system (i.e., channel floor, overbanks, lobe, and distal flat basin). We also build on previous work on repeated bathymetric surveys and core dating (Heijnen et al., 2022; Syvitski et al., 1988) to derive SRs and OC burial fluxes across the fjord.

3. Materials and Methods

3.1. River Sampling

We used 22 samples to characterize OC supply from the rivers. These samples cover a range of grain size classes and environments including the rivers' suspended load (i.e., filtered from the river waters; $n = 6$), the river banks ($n = 3$), the river bed ($n = 1$), the delta-top plains ($n = 4$), and the river plumes at the fjord surface ($n = 8$; Figure 2). The sampling campaign was conducted on 26 October 2017 (Figures 2 and 3; Figure S3 in Supporting Information S1), when the Homathko River discharge was 390 m^3/s (Water Survey of Canada, 2020). This is higher than the 250 m^3/s average annual river discharge and lower than its ∼800 m^3/s average summer peak discharges (Water Survey of Canada, 2020).

3.2. Fjord Sampling and Definition of Subenvironments

Two field campaigns were conducted in June 2016 and October 2016 to sample the fjord sediments. In total, we use a set of 15 sediment cores, which sampled the upper 30–200 cm of seabed sediment. These cores were located across all subenvironments of the fjord's seabed, including the sandy channel floor and lobe, as well as the muddy overbank and distal flat basin (Figure 3). We have few constraints on the characteristics/extent of turbidity current overbank flows, so we infer the overbank's external limit as the base of the fjord walls (red outlined area in Figure 3). We note that sediment cores from these overbank areas are located relatively close to the sandy channel. A sediment core at the end of the fjord (650 m water depth) is used to characterize the OC composition for the entire distal flat basin (core 15; light blue outlined area in Figure 3). We have no samples on the steep fjord sidewalls; hence, these areas are not included in our OC analyses.

Logging of the sediment cores allowed sandy and muddy facies to be identified (Figures 3e and 3f). A total of 99 subsamples were collected from the fjord sediment cores, to ensure representative sampling of each of the facies that were present in the channel floor, overbanks, lobe, and distal flat basin. All samples were analyzed for carbon geochemistry, as described below.

3.3. Geochemistry on River and Fjord Samples

Total carbon (TC) was measured on all river and fjord samples using an LECO elemental analyzer. All samples were also analyzed for total organic carbon (TOC) content after trace amount of inorganic carbon (carbonate) was removed using HCl and rinsing with milli-Q water. No effervescence was observed during this acidification step, confirming minimal carbonates in the system (Figure 4). TOC measurements allowed for quantifying the total amount of OC delivered by the rivers and buried in the different fjord subenvironments (Figure 5). In order to constrain the type (terrestrial or marine) of OC, all samples were analyzed for carbon stable isotopes ($\delta^{13}C$) using an isotope ratio mass spectrometer (Figure 6). Terrestrial organic matter derived from C3 plants has an average $\delta^{13}C$ between −26‰ and −28‰ (Hecky & Hesslein, 1995) and can reach values as low as −31‰, which correspond to young woody debris (Hage et al., 2020). In contrast, marine organic matter preserved in northeast Pacific sediments has an average $\delta^{13}C$ of −21.5‰ (MacDonald et al., 1991).

Previous work in Bute Inlet has used a wider range of methods (e.g., radiocarbon $\Delta^{14}C$ dating and separation of OC mixtures by ramped pyrolysis–oxidation [RPO]) on selected river and sandy channel samples (Hage et al., 2020). We complement these previous detailed measurements with new ^{14}C and RPO measurements on three samples

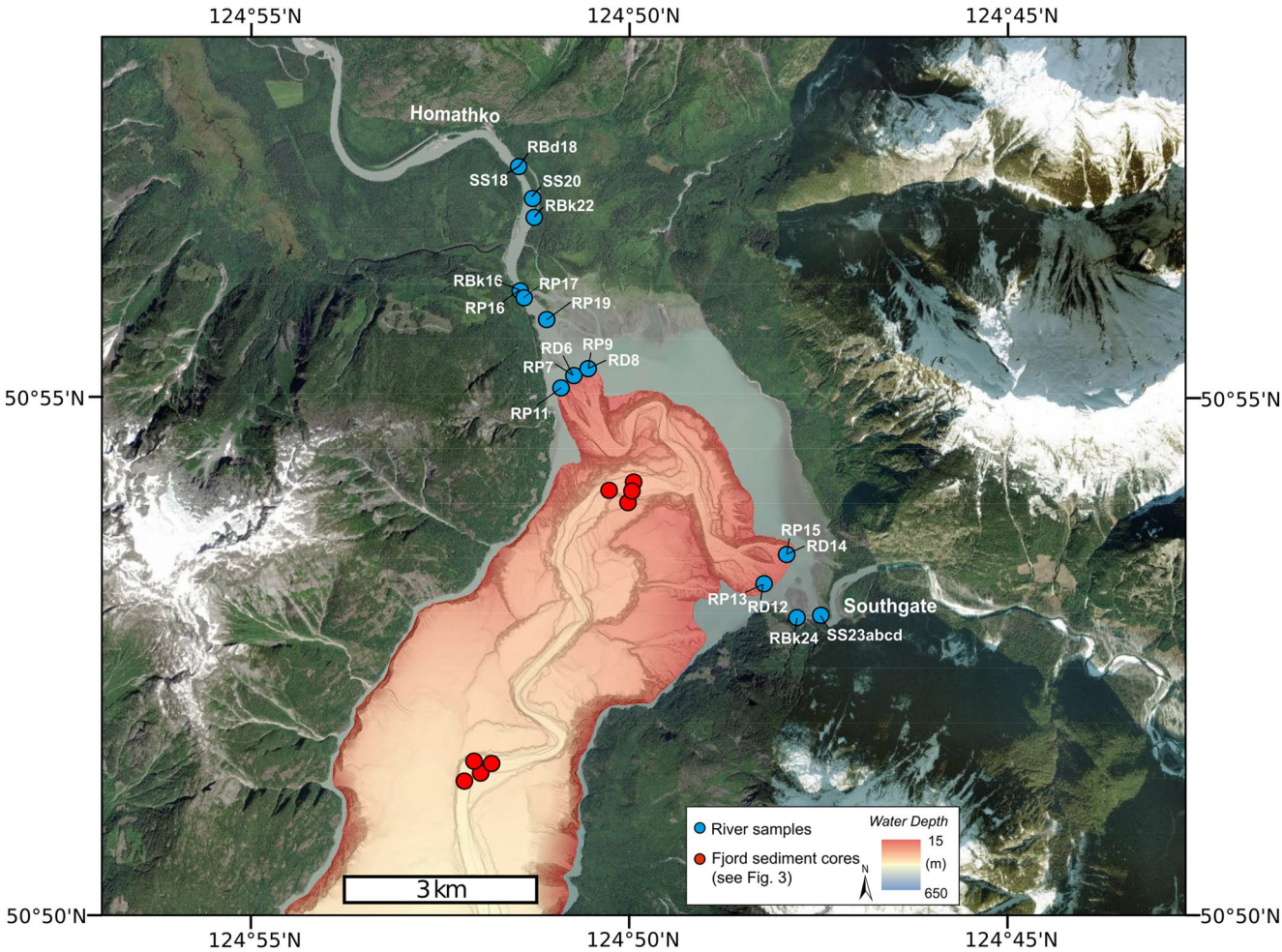

Figure 2. Bathymetry of the head of Bute Inlet (collected in 2008 by the CCGS Vector), also showing locations of sediment samples collected in Homathko and Southgate Rivers in 2017 (blue dots), and offshore in fjord sediments in 2016 (red dots). Sample codes denote the type of samples collected in rivers: RBd, river bed; SS, suspended sediment; RBk, river bank; RP, river plume; RD, river delta.

from the distal subenvironment (Figure 7). The RPO method identifies OC fractions based on thermal lability by heating each sample from 20°C to 1000°C in an oxygenated carrier gas, thus sequentially combusting OC into CO_2. The CO_2 collected between temperature intervals ("fractions") is measured for carbon stable isotopes ($\delta^{13}C$) and radiocarbon activity ($^{14}C/^{12}C$). These isotope measurements on separated fractions enabled characterization of the distribution of OC source and age within individual samples (Hemingway et al., 2017).

3.4. Calculation of River OC Fluxes

In order to determine the particulate OC fluxes from rivers, we use bedload sediment discharge data published in past literature (Syvitski & Farrow, 1983, Text S2 in Supporting Information S1), recent total suspended sediment measurements conducted on the Homathko and Southgate Rivers (Text S3 in Supporting Information S1), and TOC measurements of river sediments collected in October 2017 (Table 1).

Bedload discharge for the Homathko River was estimated at 3,100 Kt/year by Syvitski and Farrow (1983). We scaled this Homathko bedload estimate to the Southgate River using the ratio of watershed areas (Table 1; Text S2 in Supporting Information S1). The yearly mean suspended load discharge for the Homathko and Southgate Rivers was estimated at 7,946 and 221 Kt/year, respectively. This is based on suspended samples collected approximately monthly between 2018 and 2021 for the Homathko River (Text S3 in Supporting Information S1), together with daily water discharge data (Runkel et al., 2004; Text S3 in Supporting Information S1). There was no water

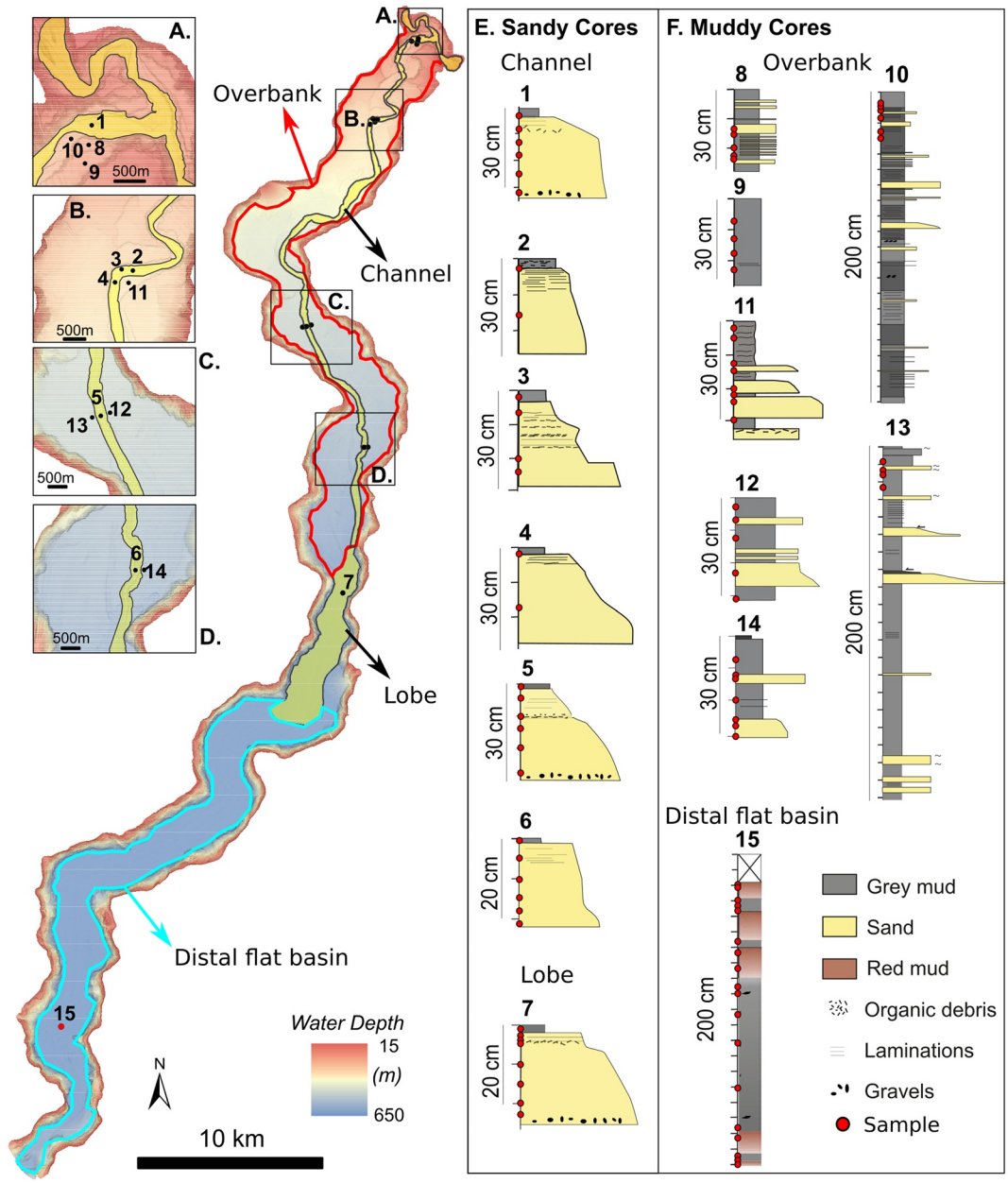

Figure 3. Submarine morphology and sediment cores collected in the Bute turbidity current system. (a–d) Zoom-ins showing the parts of the system bounded by overbank. (e, f) Sediment core set; 30-cm-long cores were collected using a box coring system; 200-cm-long cores were collected using a piston coring system.

discharge data available for the Southgate River up to 2021. Therefore, a linear regression was used to estimate daily Southgate River water discharge from Homathko River discharge, similar to Hood et al. (2020). The training data set contained 123 daily flow observations spanning a broad range of flows from record high discharge in late June 2021 through moderately low flows in October 2021 (Text S1 in Supporting Information S1).

Finally, we derived each of the river OC fluxes by multiplying the average percent TOC of river bedload and suspended load samples by the annual bedload and suspended sediment discharge, respectively (Table 1). The percent TOC of the bedload is the average between percent TOC measured on coarser samples collected in the river bed, the river banks, and the river deltas.

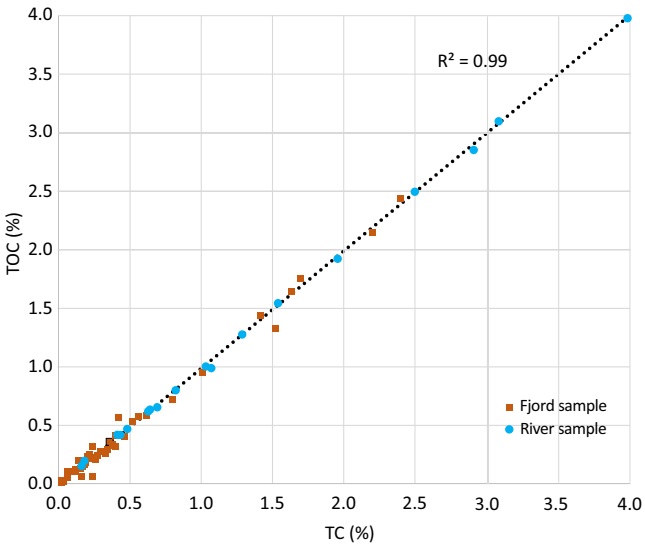

Figure 4. Comparison between total carbon (including inorganic and organic carbon) and total organic carbon content measured on all samples collected in rivers and fjord.

3.5. Calculation of OC Burial Rates in Fjord Sediments

The OC burial rates (Kt/year) in the fjord are calculated using Equation 1 (Table 2; Baudin et al., 2020) as follows:

$$\boldsymbol{A}\times\mathbf{TOC}\times\boldsymbol{\rho}\times(\mathbf{1}-\boldsymbol{\phi})\times\mathbf{SR}, \quad (1)$$

where A is the surface area of a subenvironment (m^2), TOC is the total OC content (%) averaged between samples from a given subenvironment, ρ is the grain density (kg/m^3), φ is the porosity (%), and SR is the sedimentation rate (m/year).

SRs typically vary when measured over different timescales (Sadler, 1981), especially in a highly active turbidity current system (Heijnen et al., 2020; Prior et al., 1987), making them challenging to quantify. Thus, SRs were estimated herein based on two independent approaches that provide ranges of SRs (Texts S4 and S5 in Supporting Information S1).

The first approach uses differences between two bathymetric surveys obtained in 2008 and 2018 and thus holds for a decennial timescale (Heijnen et al., 2022; Table 2 and Text S4 in Supporting Information S1). This approach highlights zones of erosion and deposition that migrate upstream significantly (100–450 m per year) due to the presence of active knickpoints in the channel (Heijnen et al., 2020). This explains why the channel is net erosive on a decennial timescale (SR = ∼−16 cm/year). The 30-cm-long sediment cores used in this study thus probably represent deposits that were a few days to weeks old, as direct monitoring shows that over 100 turbidity currents can occur in one freshet (Chen et al., 2021; Pope et al., 2022). The top of these deposits was likely reworked again by turbidity currents in the following days to weeks, progressively moving the sediment down the channel. The channel thus acts as a conduit through which sand and associated OC is shuffled to the lobe, in multiple stages over several weeks to several decades (Heijnen et al., 2022). Time-lapse bathymetry also shows that the terminal lobe is built up from a small number of large magnitude "channel flushing" events (Heijnen et al., 2022), resulting in a locally high SR (SR = 18 cm/year, Table 2) over decennial timescales. It should be kept in mind that this bathymetric method underestimates the depositional volume in areas of slow deposition (overbanks), as cm-thin drapes of sediment cannot be resolved by this method.

The second approach uses ^{210}Pb and ^{137}Cs dating methods applied to sediment cores collected in the Bute Inlet overbank and distal flat basin settings (Heerema, 2021; Syvitski et al., 1988; Text S5 in Supporting Information S1) and thus holds for a centennial timescale. This approach postulates that the entire Bute submarine system is net aggrading over centennial timescales, with SR in the overbanks and distal flat basin being 2 ± 1.5 and 1 ± 0.5 cm/year, respectively (Syvitski et al., 1988). ^{210}Pb and ^{137}Cs dating was not possible in the channel and lobe subenvironments as they are too sandy. Instead, we used an assumed relationship between the SR obtained in the overbank and that of the channel and lobe (Equations S4 and S5 in Supporting Information S1; Baudin et al., 2020). Thus, the channel floor is assumed to aggrade at a slow, but positive SR (SR = 0.7 ± 0.5 cm/year), rather than being strongly erosional. This is consistent with a rather shallow (∼20 m relief) channel, as prolonged erosion in a submarine channel that is likely at least hundreds of years old would have carved a much deeper conduit. This slow, but positive, SR in the channel is then assumed to be balanced by less aggradation in the lobe (SR = 10 cm/year; Equation S5 in Supporting Information S1).

In total, we use ranges of SRs for each subenvironment as follows. SR in the channel ranges from −16 cm/year (i.e., erosional) to 0.7 cm/year (i.e., slightly depositional). SR in the lobe ranges from 10 to 18 cm/year, implying a large accumulation of sediment over both decennial and centennial timescales. SR in the overbank area varies between 2 and 2.3 cm/year. Finally, SR in the distal flat basin ranges from 1 to 2.3 cm/year.

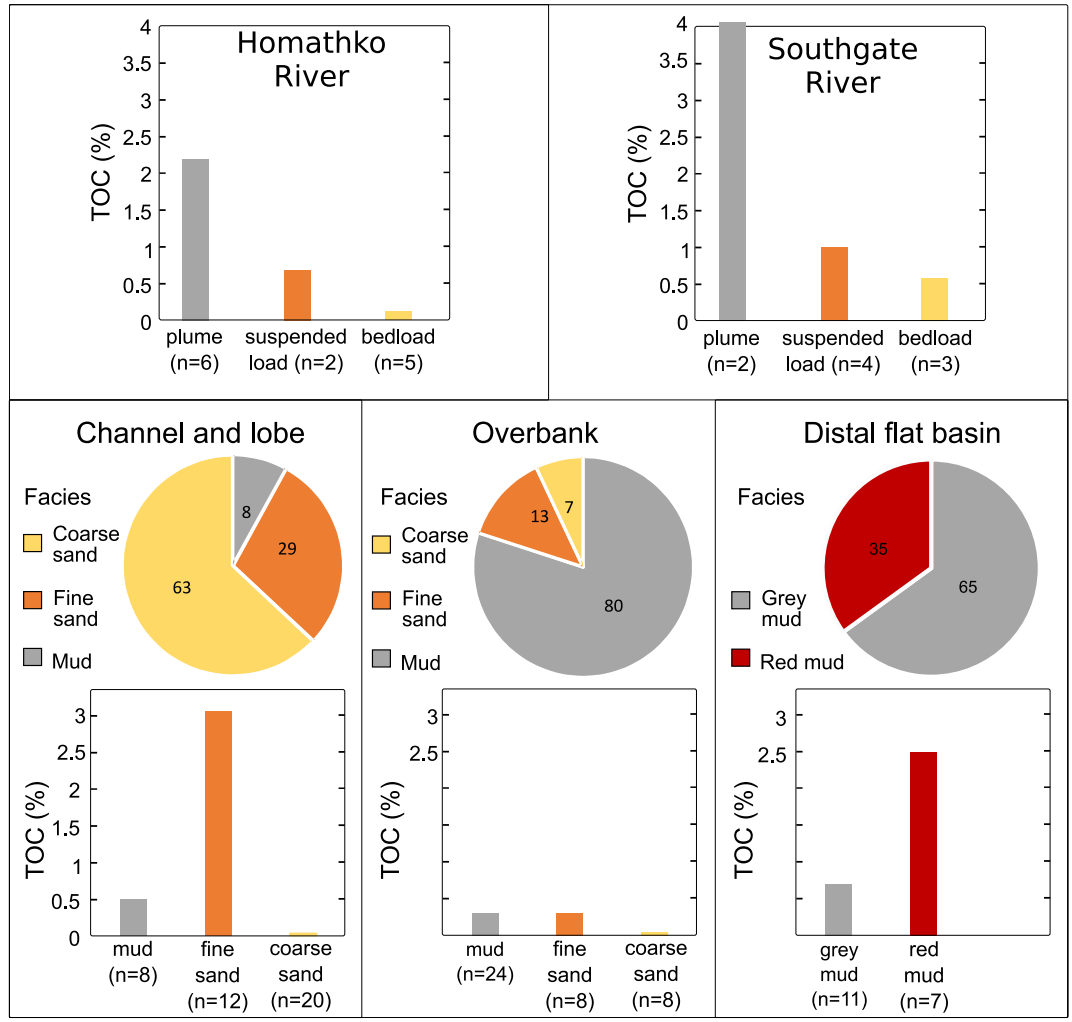

Figure 5. Facies and total organic carbon (TOC) content within rivers, submarine channel and lobe, overbank, and distal flat basin. Pie charts represent the contribution (in %) of each of the facies to a given subenvironment. The TOC content of the river "bedload" includes samples collected in the river bed, banks, and deltas.

4. Results

Below we provide the OC content and composition for both rivers and the fjord sediments separately. We note that comparison between TC and TOC on all samples revealed the absence of carbonates within both river and fjord samples (Figure 4).

4.1. Carbon Composition Supplied by Both Rivers; What Is Coming In?

Coarse sand samples collected from the riverbank and delta areas have relatively low TOC (mean TOC = 0.35%; Table S7 in Supporting Information S1), and $\delta^{13}C$ values (−27‰ to −28‰) indicating a terrestrial origin (Hecky & Hesslein, 1995). TOC is moderately high (mean TOC = 0.8%; Table S7) in the fine sands sampled from the river suspended load, banks, and deltas; whereas $\delta^{13}C$ values are low (−25‰ to −29‰) and point again to a terrestrial origin (Hecky & Hesslein, 1995). TOC is highest in muddy sediments (mean TOC = 3.1%, Figure 5) collected in the river plume at the fjord head. $\delta^{13}C$ signatures for these river plume samples are unusually high (−12 to −20 ‰; Figure 6), despite the absence of carbonates (Figure 4). These high $\delta^{13}C$ values are interpreted to be linked to bacterioplankton producing extracellular polymeric substances (EPS; Albright, 1983), and this will be further discussed in Section 5.1.

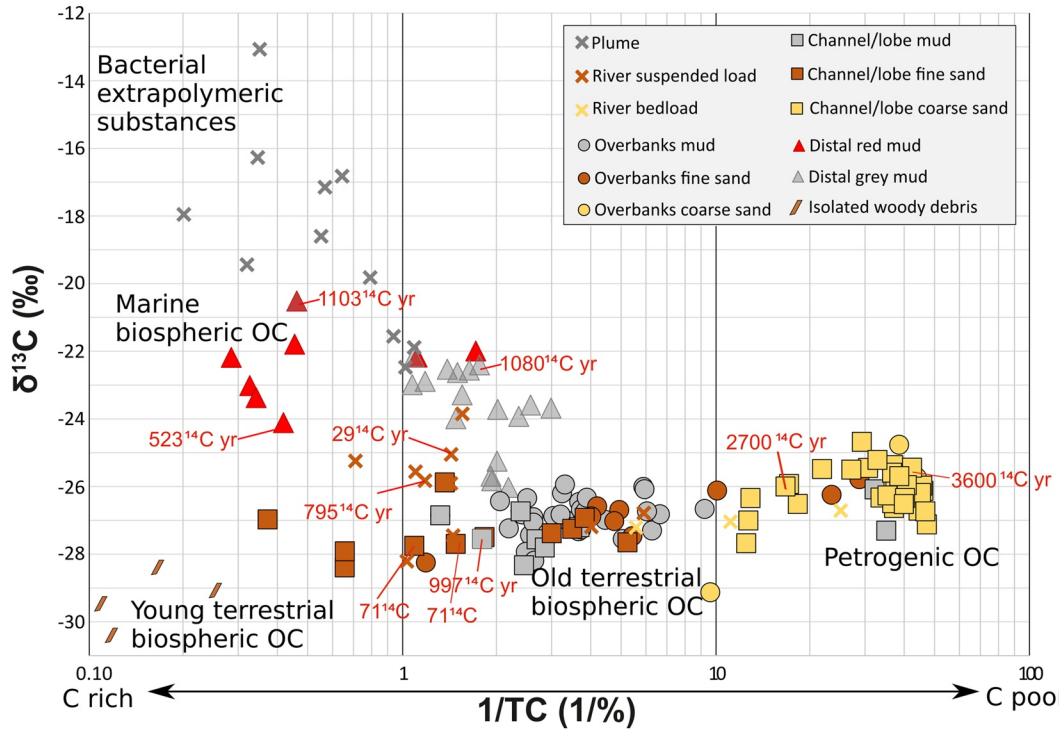

Figure 6. Total carbon (TC) content versus carbon stable isotopes ($\delta^{13}C$) measured on all samples collected in the rivers and in the Bute turbidity current system. $\delta^{13}C$ values are reported relative to Vienna Pee-Dee Belemnite (VDBP). Radiocarbon dates are expressed as reservoir age offsets in ^{14}C years (following Soulet et al., 2016). The combination of bulk measurement of carbon, stable isotopes, and radiocarbon isotopes allowed five carbon pools to be identified. (a) Extra polymeric substances associated with bacterioplankton in the river plumes at the surface of the fjord waters (Albright, 1983). (b) Marine carbon produced in the distal site. (c) Young terrestrial carbon in the form of woody debris almost exclusively buried in the sandy submarine channel. (d) Old terrestrial biospheric organic carbon aged in soils. (e) Petrogenic (rock-derived) organic carbon associated with coarse sand.

In total, we estimate that about 22.7 ± 13.1 Kt OC/year are delivered annually by the Homathko and Southgate Rivers. This is based on the estimated sediment discharge (suspended and bedload) and on the average TOC content measured between samples collected in both rivers in October 2017 (Table 1).

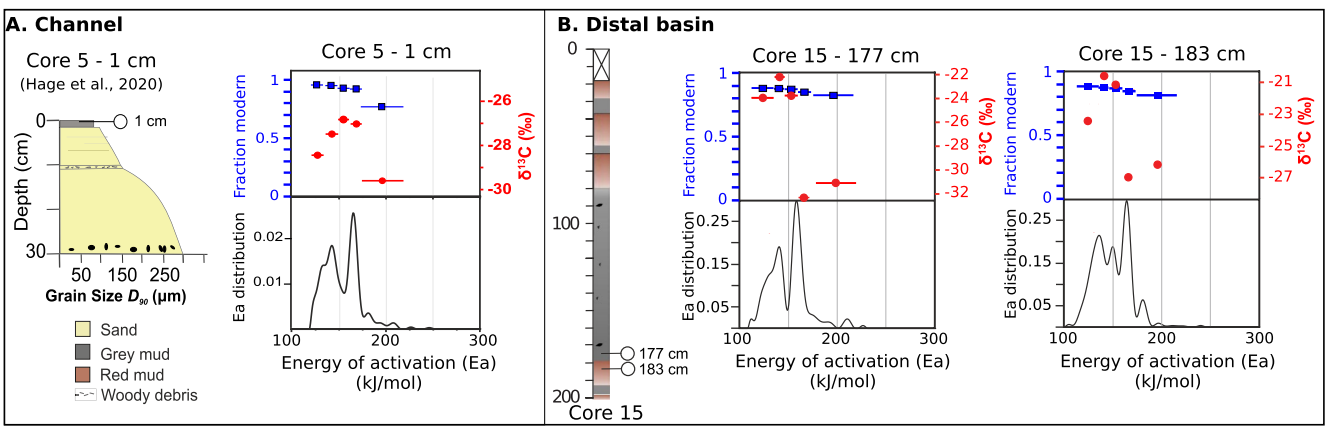

Figure 7. Separation of organic carbon (OC) mixtures by ramped pyrolysis–oxidation (RPO) and carbon isotopes measurements on separated fractions. (a) RPO analysis on a mud sample collected in the submarine channel (presented in Hage et al., 2020). (b) RPO analysis on two mud samples collected in the distal flat basin (core 15 in Figure 3). Black lines show distribution of activation energy (E_a; thermogram; Hemingway et al., 2017). Blue squares show radiocarbon ages (in fraction modern, Fm, a measurement of the deviation of the $^{14}C/^{12}C$ ratio of a carbon fraction from "modern"). Red dots show carbon stable isotopes ($\delta^{13}C$, in ‰). Blue bars represent the E_a range to which each red dot and blue square applies.

Table 2
Sediment Budget and Organic Carbon (OC) Fluxes in the Subenvironments of the Bute Turbidite System Over 10 and 100 Years Timescales

	Channel floor		Lobe		Overbank		Distal basin		Total submarine system	
	10 years	100 years	10 years	100 years	10 years	100 years	10 years	100 years	10 years	100 years
Surface area (m^2)	12.2×10^6		15.4×10^6		77.0×10^6		58.0×10^6		163×10^6	
Sedimentation rate (m/year)	−0.16[a]	0.007[b]	0.18[a]	0.1[b]	0.023[a]	0.02[c]	0.023[a]	0.01[c]		
Sedimentation rate error (m/year)	−0.09	0.005	0.22	0.050	0.006	0.015	0.006	0.003		
Sediment volume budget (Mm^3/year)	−2.0[a]	0.1	2.73[a]	1.5	1.8	1.5	1.3	0.6	3.8	3.7
Sediment volume budget error (Mm^3/year)	−1.09	0.06	3.45	0.8	0.46	1.1	0.35	0.17	3.2	2.2
% coarse sand	63		63		7		0			
% fine sand	29		29		13		0			
% gray mud	8		8		80		65			
% red mud	0		0		0		35			
TOC in coarse sand (%)	0.03		0.03		0.04		0			
TOC in fine sand (%)	3.2		3.2		0.3		0			
TOC in gray mud (%)	0.5		0.5		0.3		0.7			
TOC in red mud (%)	0		0		0		2.5			
TOC weighted with facies (%)	1		1		0.3		1.3			
Porosity (%)	70		70		80		85			
Grain density (kg/m^3)	2,585		2,585		2,585		2,585			
OC flux (Kt OC/year)	−15.6	0.7	21.2	11.9	2.9	2.4	6.8	2.9	15.4	17.9
OC flux error (Kt OC/year)	−8.5	0.5	26.9	5.9	0.8	1.7	1.2	0.9	20.3	9.1
Terrestrial OC flux (Kt OC/year)	−15.6	0.7	21.2	11.9	2.9	2.4	3.1	1.3	11.7	16.3
Terrestrial OC flux error (Kt OC/year)	−8.5	0.5	26.9	6.0	0.8	1.8	1.2	0.6	20.3	8.8

Note. OC annual fluxes are obtained as follows: OC flux = sediment volume × TOC × (1 − porosity) × density.

[a]Sediment volumes derived from repeated bathymetric surveys between 2008 and 2018 (Heijnen et al., 2022). Sedimentation rates are obtained by dividing the sediment volume by the surface area of a given subenvironment. Volume uncertainties are based on vertical accuracy of the multibeam surveys of 0.5% of the water depth. Hence, the 600-m-deep lobe is greatly affected (Heijnen et al., 2020). [b]Assumed sedimentation rates in the channel and lobe are based on c and Baudin et al. (2020); see Supporting Information S1. [c]100 years sedimentation rates in the overbank and distal basin are based on ^{210}Pb and ^{137}Cs dating (Syvitski et al., 1988; Heerema, 2021; Supporting Information S1).

4.2. Facies and Carbon Composition in the Fjord; What Is Preserved and Where?

We now present the OC content and composition within the fjord seabed, across the four previously defined subenvironments (Figure 3).

Sediment cores collected from the sandy *channel floor* and *lobe* have similar facies and OC composition (Figure 3, Table S7 in Supporting Information S1), thus the OC composition of these subenvironments is described together. The channel floor and lobe contain 63% carbon-poor (mean TOC = <0.05%) coarse sand, 29% carbon-rich (mean TOC = 3%) fine sand, and 8% carbon-moderate (mean TOC = 0.5%) mud (Figure 5). $\delta^{13}C$ and ^{14}C ages revealed that fine sands contain young terrestrial woody debris (visible to the naked eye), buried under older biospheric soil organic matter in the muds (Hage et al., 2020; Figure 6).

In contrast to the channel floor and lobe, the *overbanks* are dominated (80%) by muddy deposits characterized by lower TOC values (0.35% on average; Figure 5). Fine sands found in the overbank cores have much lower TOC values compared to fine sands in the channel floor and lobe. $\delta^{13}C$ signatures range between −26‰ and −28‰, pointing to a terrestrial origin of the organic matter (Figure 6). We note the absence of woody debris visible to the naked eye in the overbank cores, as opposed to the channel floor and lobe cores.

The top 2 m of sediment recovered from the *distal flat basin* is made exclusively of muddy sediments characterized by homogeneous red (35%) or gray facies (65%). Gray muds have moderate TOC (0.65% on average; Figure 5) and a wide range of $\delta^{13}C$ signatures, suggesting a mixed terrestrial and marine origin of organic matter

(−22‰ to −26‰; Figure 6). Red muds have high TOC (2.5% on average; Figure 5) with $\delta^{13}C$ between −20.5‰ and −23‰ (Figure 6) that point to a marine-dominated origin (MacDonald et al., 1991). Based on a binary mixing model using $\delta^{13}C$ compositions of marine (−20.5‰) and terrestrial (−27‰, Hecky & Hesslein, 1995) OC end-members, we estimate that about 54% of the OC found in the upper 2 m of sediment on the distal flat basin is of marine origin (Text S6 and Table S6 in Supporting Information S1). ^{14}C data and RPO thermograms on the red and gray muds in this distal site (Figure 7) reveal that the OC in this muddy distal site is of similar age (500–1,100 ^{14}C years), compared to the organic matter found in the muddy deposits of the channel (997 ^{14}C years; Figure 6, Hage et al., 2020). Overall, OC associated with muds in the active channel and distal flat basin are older compared to the young OC associated fine sands found in the active channel (Figure 6, Hage et al., 2020).

In total, we estimate that the top 2 m of sediments in the Bute turbidity current system have an annual OC burial rate ranging from 15.4 to 17.9 Kt OC/year over decennial to centennial timescales, respectively (Table 2). We divide this budget between terrestrial and marine OC contribution based on the mixing model applied to the distal flat basin samples (Text S6 in Supporting Information S1). In total, between 11.7 and 16.3 Kt OC/year of terrestrial origin carbon are found in the fjord, in all of its subenvironments. Between 1.6 and 3.7 Kt OC/year of marine origin carbon are found in the distal flat basin (Figures 6 and 7 and Table 2).

5. Discussion

5.1. How Much Particulate OC Is Delivered by the Two Rivers Discharging Into Bute Inlet?

We have estimated that Homathko and Southgate Rivers carried 22.7 ± 13.1 Kt OC/year into Bute Inlet based on suspended and bedload sampling conducted in 2017 (Table 1). This total OC flux is interpreted to contain three pools (Figure 6): young terrestrial biospheric (woody debris), old terrestrial biospheric (soil organic matter), and petrogenic OC (rock-derived OC). Identification of these pools is based on TOC and $\delta^{13}C$ signatures (Figure 6), and on ramped oxidation data combined with radiocarbon dates previously presented in Hage et al. (2020). To these three pools previously identified, we add a fourth pool made of EPS associated with bacterioplankton that occurs when the rivers enter the fjord and create surface plumes in which the heterotrophic activity of bacterioplankton can be enhanced (Albright, 1983). This activity appears to result in an OC pool characterized by high TOC (>3%) and unusually high $\delta^{13}C$ signatures (Figure 6). Such signatures cannot be explained by the presence of carbonates (typically enriched in $\delta^{13}C$) because they were removed prior to isotope measurements. These high $\delta^{13}C$ signatures may also correspond to C4 plants, yet C4 plants are almost exclusively found in tropical and warm environments (Hecky & Hesslein, 1995). The EPS hypothesis is further supported by the stickiness of the plume samples (i.e., samples sticking to the filters), which is typical for EPS (Underwood et al., 1995). This fourth pool of OC is not included in our OC river input flux as it is most likely formed within the fjord water. Further research on the highly enriched $\delta^{13}C$ composition of these plume samples is required, yet it is beyond the scope of this study. We further note that the EPS-related OC pool is not found in the fjord seabed sediment samples (Figure 6). We propose this is because OC associated with EPS is labile and not heavy enough to settle, and it thus degrades rapidly in the water column before reaching seabed sediments (Albright, 1983).

We note that there are key assumptions behind these estimates of riverine OC composition. First, we have a limited number of riverine OC samples ($n = 22$) and these samples were collected during a rain-induced runoff event in fall when river discharge was near the annual average (Text S1 in Supporting Information S1). River discharge peaks driven by the freshet and/or intense rain likely brought more and coarser terrestrial organic debris than the rates estimated here (as in Turowski et al., 2016). We thus expect these river OC fluxes to fluctuate following extreme events such as floods, yet the data presented in this study do not constrain this variability. Second, we have no constraints on the OC content potentially coming from small streams entering the fjord along its margins. However, these streams only represent 6% of the total sediment and freshwater input coming into the fjord (Syvitski & Farrow, 1983).

5.2. How Much and What Type of OC Is Buried in the Bute Inlet Subenvironments?

The surficial sediments from the Bute turbidity current system bury a total of 15.4–17.9 Kt OC/year, with 11.7–16.3 Kt OC/year being of terrestrial origin. Thus, 76%–91% of the OC buried in Bute Inlet is terrestrial. This proportion is higher than previous estimates made in other fjords where 42%–65% of the OC was found to be terrestrial (Cui, Bianchi, Jaeger, et al., 2016; Cui, Bianchi, Savage, et al., 2016; Smeaton & Austin, 2019),

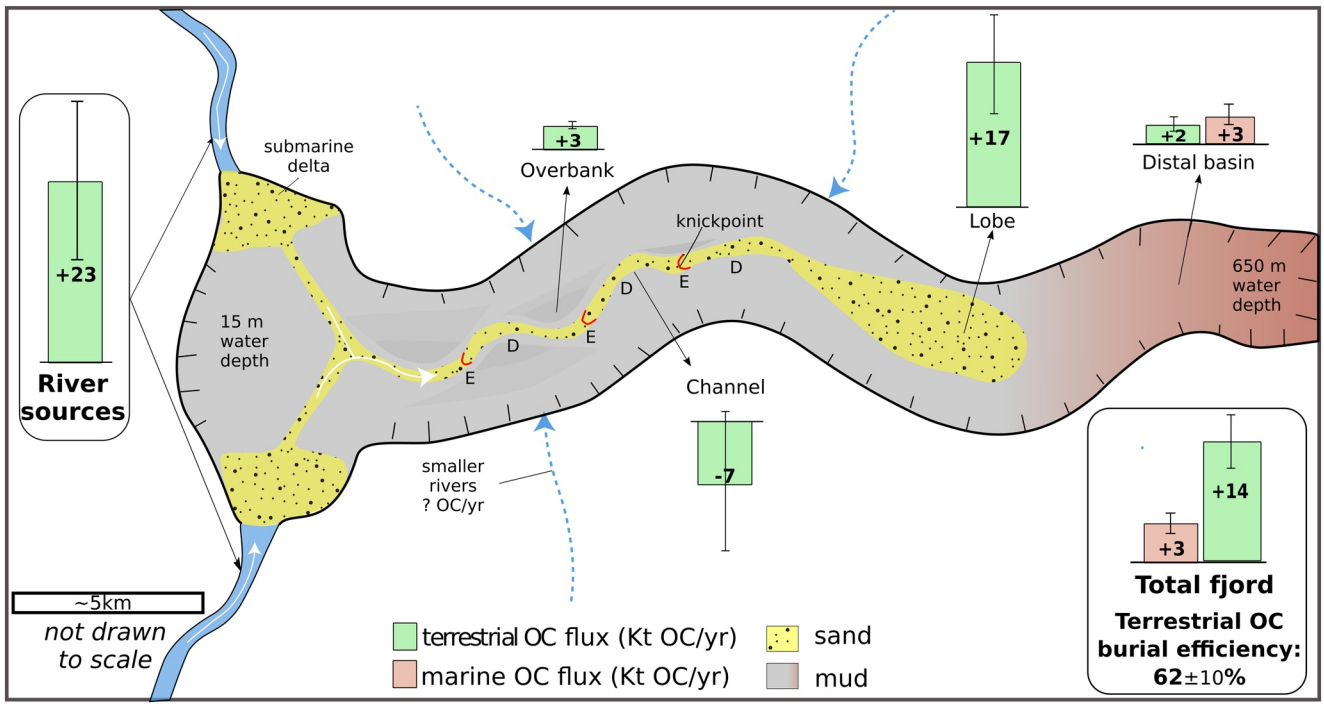

Figure 8. Summary illustration (not to scale) showing total organic carbon (OC) fluxes from rivers to seafloor sediment in Bute Inlet. OC fluxes are given as the average value between sediment budgets estimated using two approaches covering two timescales (i.e., decade to century; see Section 3; Heerema, 2021; Heijnen et al., 2022; Syvitski et al., 1988). Error bars correspond to the range between the two approaches. Sediment and OC are shuffled stepwise down the channel before reaching the lobe due to migrating knickpoints. The channel is thus net erosive over decennial timescales, with patches of erosion (E) and deposition (D) between knickpoints. Over longer timescales (>100's year), the channel is interpreted as being neutral to slowly aggrading.

probably due to the lower riverine inputs compared to Bute Inlet. This highlights the importance of turbidity currents for distributing terrestrial OC in river-fed fjords and the necessity to include turbidity current processes when assessing the burial of terrestrial OC globally.

There are a number of uncertainties behind OC rates calculated in Bute Inlet. First, we do not have sediment cores in the distal parts of the overbanks, close to the fjord's sidewalls. Therefore, we extrapolate the SRs and OC composition found in the overbanks close to the channel to the entire overbank area. The more distal overbank sites may either be poorer in terrestrial OC compared to the sites close to the channel fed by the rivers or richer in OC due to smaller rivers and streams and potential landslides sourced from the steep fjord sidewalls. Second, we assume that the 30-cm-thick (i.e., maximum a few weeks old) deposits recovered from the channel are reproduced over centennial timescales despite the rapidly migrating knickpoints in the channel (Heijnen et al., 2020; Prior et al., 1987). We could expect that channel-floor fine sands, which are rich in OC, are excavated several times before reaching their ultimate burial location on the lobe, decreasing their OC content over time (Heijnen et al., 2022; Pope et al., 2022). However, we do not see any evidence of OC content decrease along the channel transect, at least over the very recent (30 cm below seafloor) deposits observed in this study. We suspect that the channel is an efficient conduit for the delivery of terrestrial OC to the lobe, but this needs to be confirmed with longer sediment cores that are difficult to collect in sandy channel floors (as piston corers tend to fail to penetrate sandy seabed).

Despite these uncertainties, the data collected in Bute Inlet allow us to derive for the first time a detailed OC burial budget in fjord sediments controlled by turbidity currents (Figure 8). Because the channel is net-erosional (i.e., negative OC flux, Figure 8, Table 2) and is balanced by deposition on the lobe over a decadal timescale (i.e., any material in the channel will ultimately be shuffled and buried on the lobe, Heijnen et al., 2022), we provide a combined OC burial contribution for these two environments. Together the channel and lobe, dominated by sands (Figures 3 and 5, Table S7 in Supporting Information S1) and only covering 17% of the fjord's seafloor area (Table 2), comprise 48%–77% of the total annual terrestrial OC burial flux in Bute Inlet. This terrestrial OC is predominantly young, associated with fine sands and buried beneath a layer of mud including old biospheric

OC (Hage et al., 2020; Figure 7). The overbanks, dominated by mud (Figure 5) and covering 47% of the fjord's seafloor area, comprise 15%–25% of the total annual terrestrial OC burial flux, with low TOC in the fine sands. The settling velocities of waterlogged woody debris have been shown to be relatively rapid due to their size and density (Hoover et al., 2010; A. McArthur et al., 2016; A. D. McArthur et al., 2016; Waterson & Canuel, 2008), such that this woody debris is carried mainly along the channel floor. This concentration of woody debris along the channel floor could explain the low TOC values seen within the fine sands of the overbanks. The distal flat basin, exclusively made of mud in the surficial (200 cm) sediment and covering 36% of the fjord's seafloor area, comprises the remaining 6%–22% of the total annual terrestrial OC burial flux. The abundance of mud in the surficial sediment of the distal flat basin is explained by the limited number of turbidity currents reaching this site in present times (Chen et al., 2021; Pope et al., 2022; Prior et al., 1987).

5.3. What Is the Terrestrial OC Burial Efficiency of Bute Inlet and How Does It Compare With Other Fjords?

Comparison between OC river input (22.7 ± 13.1 Kt OC/year; Table 1) and terrestrial OC burial rate (11.7–16.3 Kt OC/year; Table 2) suggests that Bute Inlet has a terrestrial OC burial efficiency ranging between 52% and 72% (62% ± 10% on average) when estimated over decennial and centennial timescales, respectively.

No study has closed budgets between river sources and fjord sediments before, so it is not possible to compare this value with other river-fed fjords. However, we can compare our results in Bute Inlet with previous fjord studies, by normalizing OC burial rates to Bute Inlet's total surface area. By doing so, the burial of terrestrial OC in Bute Inlet ranges between 72 and 100 t C/km^2/year. This range lies between previous estimates of area-normalized OC fluxes of 57–107 t C/km^2/year in Scottish and Irish fjords that were described as having heterogeneous seafloors (Smeaton & Austin, 2019). Our results from Bute Inlet suggest that fjords characterized by sandy turbidity current systems may bury over 3 times more terrestrial OC compared to global estimates (22 t C/km^2/year; Cui, Bianchi, Jaeger, et al., 2016; Cui, Bianchi, Savage, et al., 2016; Smith et al., 2015) based on muddy cores from fjords without any identified turbidity current channels (and usually lacking multibeam surveys). It was previously shown that turbidity currents are more active in fjords that are characterized by larger riverine inputs, steeper and deeper offshore slopes (Gales et al., 2019; Pope et al., 2019). Such factors need to be carefully considered when assessing OC burial potential in fjords.

5.4. Comparison With Larger, Deep-Sea Turbidity Current Systems

To our knowledge, only one study has provided OC balance budgets between river source and turbidity current subenvironments within a single system. This is the Congo River to the Congo Fan (Baudin et al., 2017, 2020; Coynel et al., 2005), where burial rates are calculated over centennial timescales that are comparable to the longer timescales considered in this study. Using a source to sink approach, Baudin et al. (2020) found that 33%–69% of the annual OC delivered by the Congo River is buried in the Congo turbidity current system. This burial efficiency is similar to, if slightly lower than, our estimate in Bute Inlet (52%–72%), highlighting the difficulty in closing budgets between river source and marine sinks fed by turbidity currents (Baudin et al., 2020). Within these two turbidity current systems, both the Congo and Bute Inlet submarine canyon-channels show minimal long-term (>100 years) OC accumulation, potentially indicating remineralization of the OC. However, remineralization was shown to occur in small proportions in the Congo system, based on in situ measurements of total oxygen uptake made on the lobe sediments (Rabouille et al., 2019). Finally, we note that undersampling of the Congo Canyon and Channel occurred in past studies due to the difficulty with sampling sandy deposits (Baudin et al., 2020). This undersampling of the canyon and channel may result in underestimation of OC burial rates in the Congo Channel, similar to the Bute Inlet channel where only 30-cm-long sediment cores could be retrieved. In both Congo and Bute Inlet systems, the lobe holds most of the total buried OC.

Besides this example from the Congo system, work in Gaoping Canyon offshore Taiwan shows a terrestrial OC preservation efficiency of >70% in marine sediments. The Gaoping submarine canyon is supplied by river floods (hyperpycnal) and dilute surface plume (hypopycnal) inputs (Kao et al., 2014). This high OC burial efficiency results from Taiwan being a mountainous island and a hotspot for sediment and OC production, with frequent typhoon-generated floods and turbidity currents that deliver terrestrial OC (e.g., woody debris associated with sands) through the submarine canyon to the deep-sea (Hilton et al., 2008; Liu et al., 2016; West et al., 2011).

Another example of high OC burial efficiency comes from the Bay of Bengal where almost no loss of OC was observed between the Ganges–Brahmaputra River inputs and the Bengal Submarine Fan (Galy et al., 2007). Coarse turbidity current deposits from the channel-levees of the Bengal Fan submarine system were also shown to have abundant terrestrial woody fragments throughout the last 19 Myr (Lee et al., 2019). These OC-rich turbidity current deposits are interpreted to result from turbidity currents triggered by high-magnitude, low-frequency events (e.g., floods, cyclones; Lee et al., 2019).

Based on these examples, it is plausible that rare and extreme events may also affect the OC burial efficiency and distribution in Bute Inlet, potentially increasing our burial efficiency estimate. It was recently shown that most turbidity currents (~90%) dissipate within the shallowest-water (<200 m depth and <12 km along channel from the Homathko Delta) part of Bute Inlet, whereas less frequent (~10%) events rework this material and progressively shuffle it downstream to the lobe (Heijnen et al., 2022; Pope et al., 2022). We further suspect that rare long runout events can flush material to the distal flat basin, as evidenced by thick sandy accumulations found at >3 m depth in 8-m-long piston cores collected in the distal basin at the location of core 15 (Figure 3, Heerema, 2021). Based on our OC burial efficiency estimates (i.e., 50%–70% over decennial to centennial timescales, respectively), it appears that OC burial efficiency is higher when considering longer timescales, which are more likely to integrate some higher magnitude, less frequent events than shorter timescales.

An example of a rare and large event occurred in the Bute Inlet catchment on 28 November 2020 when a glacial lake outburst flood took place at Elliot Creek, which is a tributary of Southgate River (Figure 1). This outburst flood—caused by an exceptionally large landslide—discharged about 4 million m^3 of terrestrial sediment (including soil organic matter) and a large volume of woody debris into the Southgate River and ultimately Bute Inlet (Geertsema et al., 2022). The impact of this event on the OC burial in Bute Inlet is yet to be determined and compared with the preevent OC fluxes presented in this study, but it may help to understand sediment and OC delivery in infrequent but large magnitude events.

6. Conclusion

This study provides the first complete source to sink budget for OC in a river-fed fjord turbidity current system, showing how OC is distributed within the upper <2 m of sediment. OC fluxes are estimated for the fjord's two river sources (Homathko and Southgate Rivers, which provide 94% of the water and sediment discharge to the fjord) and compared to OC burial fluxes in different seafloor subenvironments. We estimate that the annual OC export from both rivers to the fjord is 23 ± 13 Kt C/year, although this may not capture the full annual range of streamflow variability. The annual terrestrial OC burial rate of the entire fjord is estimated to range from 12 to 16 Kt OC/year. This suggests that a relatively high terrestrial OC burial efficiency (62% ± 10%) occurs within the fjord. Terrestrial OC is distributed as follows across the fjord seafloor; 63% ± 14% of the total terrestrial OC burial occurs in the sand-dominated subenvironments (covering 17% of the fjord seafloor area), whereas 37% ± 14% occurs in the mud-dominated subenvironments (covering 83% of the fjord seafloor area). Therefore, hydrodynamic fractionation of OC by turbidity currents leads to variable burial efficiencies in different subenvironments of the fjord. This study helps to understand how OC is buried within fjords over short (decennial to centennial) timescales. A comparison to other (nonfjord) turbidity current systems suggests that these systems consistently have high (50%–100%) terrestrial OC burial efficiency (Baudin et al., 2020; Galy et al., 2007; Liu et al., 2016). Turbidity current systems may thus play a globally important role in the highly efficient delivery and burial of mainly terrestrial OC, which affects atmospheric CO_2 levels over geological timescales (Berner, 1982) and food resources for modern benthic ecosystems (Włodarska-Kowalczuk et al., 2019).

Data Availability Statement

Discharge data for the Homathko River and Southgate River are available from https://wateroffice.ec.gc.ca; station 08GD004 and station 08GD010, respectively. Multibeam bathymetric data are held by the Geological Survey of Canada and Canadian Hydrographic Survey. Data and metadata associated with the sediment core and river samples can be found at https://doi.org/10.1594/PANGAEA.944382 and https://doi.org/10.1594/PANGAEA.944379.

Acknowledgments
We acknowledge that this work took place in the unceded traditional territory of the Homalco First Nation. We thank the captain and crew of the CCGS Vector (Canada) for sample collection. S.H. acknowledges funding by the IAS post-graduate grant scheme, a Research Development funds offered by Durham University, and the NOCS/WHOI exchange program. S.H. has received funding from the European Union's Horizon 2020 research and innovation program under the Marie Sklodowska-Curie grant agreement no. 899546. The field campaign and geochemical analyses were supported by Natural Environment Research Council grants NE/M007138/1, NE/W30601/1, NE/N012798/1, NE/K011480/1 and NE/M017540/1. M.J.B.C. was funded by a Royal Society Research Fellowship (DHF\R1\180166). M.A.C. was supported by the U.K. National Capability NERC CLASS program (NE/R015953/1) and NERC grants (NE/P009190/1 and NE/P005780/1). C.J.H. and M.S.H. were funded by the European Union's Horizon 2020 research and innovation program under the Marie Skłodowska-Curie grant agreement no. 721403 - ITN SLATE. E.L.P. was supported by a Leverhulme Early Career Fellowship (ECF-2018-267).

References

Albright, L. J. (1983). Influence of river–ocean plumes upon bacterioplankton production of the Strait of Georgia, British Columbia. *Marine Ecology Progress Series*, *12*, 107–113. https://doi.org/10.3354/meps012107

Baudin, F., Martinez, P., Dennielou, B., Charlier, K., Marsset, T., Droz, L., & Rabouille, C. (2017). Organic carbon accumulation in modern sediments of the Angola basin influenced by the Congo deep sea fan. *Deep-Sea Research Part II*, *142*, 64–74. https://doi.org/10.1016/j.dsr2.2017.01.009

Baudin, F., Rabouille, C., & Dennielou, B. (2020). Routing of terrestrial organic matter from the Congo River to the ultimate sink in the abyss: A mass balance approach (André Dumont medallist lecture 2017). *Geologica Belgica*, *23*(1–2), 41–52. https://doi.org/10.20341/gb.2020.004

Berner, R. A. (1982). Burial of organic carbon and pyrite sulfur in the modern ocean: Its geochemical and environmental significance. *American Journal of Science*, *282*, 451–473. https://doi.org/10.2475/ajs.282.4.451

Berner, R. A. (1989). Biogeochemical cycles of carbon and sulfur and their effect on atmospheric oxygen over Phanerozoic time. *Palaeogeography, Palaeoclimatology, Palaeoecology*, *75*, 97–122. https://doi.org/10.1016/0031-0182(89)90186-7

Bianchi, T. S., Arndt, S., Austin, W. E. N., Benn, D. I., Bertrand, S., Cui, X., et al. (2020). Fjords as Aquatic Critical Zones (ACZs). *Earth-Science Reviews*, *203*, 103–145. https://doi.org/10.1016/j.earscirev.2020.103145

Burdige, D. J. (2007). Preservation of organic matter in marine sediments: Controls, mechanisms, and an imbalance in sediment organic carbon budgets? *Chemical Reviews*, *107*, 467–485. https://doi.org/10.1021/cr050347q

Chen, Y., Parsons, D. R., Simmons, S. M., Williams, R., Cartugny, M. J. B., Hughes Clarke, J. E., et al. (2021). Knickpoints and crescentic bedform interactions in submarine channels. *Sedimentology*, *68*, 1358–1377. https://doi.org/10.1111/sed.12886

Clare, M. A., Hughes Clarke, J. E., Talling, P. J., Cartigny, M. J. B., & Pratomo, D. G. (2016). Preconditioning and triggering of offshore slope failures and turbidity currents revealed by most detailed monitoring yet at a fjord-head delta. *Earth and Planetary Science Letters*, *450*, 208–220. https://doi.org/10.1016/j.epsl.2016.06.021

Conway, K. W., Barrie, J. V., Picard, K., & Bornhold, B. D. (2012). Submarine channel evolution: Active channels in fjords, British Columbia, Canada. *Geo-Marine Letters*, *32*, 301–312. https://doi.org/10.1007/s00367-012-0280-4

Coynel, A., Seyler, P., Etcheber, H., Meybeck, M., & Orange, D. (2005). Spatial and seasonal dynamics of total suspended sediment and organic carbon species in the Congo River. *Global Biogeochemical Cycles*, *19*(4), GB4019. https://doi.org/10.1029/2004GB002335

Cui, X., Bianchi, T. S., Jaeger, J. M., & Smith, R. W. (2016). Biospheric and petrogenic organic carbon flux along southeast Alaska. *Earth and Planetary Science Letters*, *452*, 238–246. https://doi.org/10.1016/j.epsl.2016.08.002

Cui, X., Bianchi, T. S., & Savage, C. (2017). Erosion of modern terrestrial organic matter as a major component of sediments in fjords. *Geophysical Research Letters*, *44*, 1457–1465. https://doi.org/10.1002/2016GL072260

Cui, X., Bianchi, T. S., Savage, C., & Smith, R. W. (2016). Organic carbon burial in fjords: Terrestrial versus marine inputs. *Earth and Planetary Science Letters*, *451*, 41–50. https://doi.org/10.1016/j.epsl.2016.07.003

Dyer, K. R. (1997). *Estuaries: A physical introduction*. New York, NY: Wiley-Blackwell.

Farrow, G. E., Syvitski, J. P. M., & Tunnecliffe, V. (1983). Suspended particulate loading on the macro-benthos in a highly turbid fjord; Knight Inlet, British Columbia. *Canadian Journal of Fisheries and Aquatic Science*, *40*(1), 273–288. https://doi.org/10.1139/f83-289

Gales, J. A., Talling, P. J., Cartigny, M. J., Hughes Clarke, J., Lintern, G., Stacey, C., & Clare, M. A. (2019). What controls submarine channel development and the morphology of deltas entering deep-water fjords? *Earth Surface Processes and Landforms*, *44*(2), 535–551. https://doi.org/10.1002/esp.4515

Galy, V., France-Lanord, C., Beyssac, O., Faure, P., Kudrass, H., & Palhol, F. (2007). Efficient organic carbon burial in the Bengal Fan sustained by the Himalayan erosional system. *Nature*, *450*(2007), 407–410. https://doi.org/10.1038/nature06273

Geertsema, M., Menounos, B., Bullard, G., Carrivick, J. L., Clague, J. J., Dai, C., et al. (2022). The 28 November 2020 landslide, tsunami, and outburst flood—A hazard cascade associated with rapid deglaciation at Elliot Creek, British Columbia, Canada. *Geophysical Research Letters*, *49*(6), e2021GL096716. https://doi.org/10.1029/2021GL096716

Giesbrecht, I. J. W., Tank, S. E., Frazer, G. W., Hood, E. W., Gonzalez Arriola, S. G., Butman, D. E., et al. (2022). Watershed classification predicts streamflow regime and organic carbon dynamics in the Northeast Pacific coastal temperate rainforest. *Global Biogeochemical Cycles*, *36*(2), e2021GB007047. https://doi.org/10.1029/2021GB007047

Gonzalez Arriola, S., Giesbrecht, I. J. W., Biles, F. E., & D'Amore, D. V. (2018). *Watersheds of the northern Pacific coastal temperate rainforest margin*. Campbell River: Hakai Institute Data Package.

Hage, S., Cartigny, M. J. B., Sumner, E. J., Clare, M. A., Hughes Clarke, J. E., Talling, P. J., et al. (2019). Direct monitoring reveals initiation of turbidity currents from extremely dilute river plumes. *Geophysical Research Letters*, *46*(20), 11310–11320. https://doi.org/10.1029/2019GL084526

Hage, S., Galy, V., Cartigny, M., Acikalin, S., Clare, M., Gröcke, D., et al. (2020). Efficient preservation of young terrestrial organic carbon in sandy turbidity-current deposits. *Geology*, *48*(9), 882–887. https://doi.org/10.1130/g47320.1

Hecky, R. E., & Hesslein, R. H. (1995). Contributions of benthic algae to lake food webs as revealed by stable isotope analysis. *Journal of the North American Benthological Society*, *14*(4), 631–653. https://doi.org/10.2307/1467546

Hedges, J. I., & Keil, R. G. (1995). Sedimentary organic matter preservation: An assessment and speculative synthesis. *Marine Chemistry*, *49*(2–3), 137–139. https://doi.org/10.1016/0304-4203(95)00013-h

Heerema, C. J. (2021). *Evolution of turbidity currents: New insights from direct field measurements* (Durham theses). Retrieved from Durham E-Theses Online (http://etheses.dur.ac.uk/13963/). Durham: Durham University

Heijnen, M. S., Clare, M. A., Cartigny, M. J., Talling, P. J., Hage, S., Lintern, D. G., et al. (2020). Rapidly-migrating and internally-generated knickpoints can control submarine channel evolution. *Nature Communications*, *11*(1), 1–15. https://doi.org/10.1038/s41467-020-16861-x

Heijnen, M. S., Clare, M. A., Cartigny, M. J., Talling, P. J., Hage, S., Pope, E. L., et al. (2022). Fill, flush or shuffle: How is sediment carried through submarine channels to build lobes? *Earth and Planetary Science Letters*, *584*, 117481. https://doi.org/10.1016/j.epsl.2022.117481

Hemingway, J. D., Rothman, D. H., Rosengard, S. Z., & Galy, V. V. (2017). Technical note: An inverse method to relate organic carbon reactivity to isotope composition from serial oxidation. *Biogeosciences*, *14*, 5099–5114.

Hilton, R. G., Galy, A., Hovius, N., Chen, M. C., Horng, M. J., & Chen, H. (2008). Tropical-cyclone-driven erosion of the terrestrial biosphere from mountains. *Nature Geoscience*, *1*(11), 759–762. https://doi.org/10.1038/ngeo333

Hilton, R. G., & West, A. J. (2020). Mountains, erosion and the carbon cycle. *Nature Reviews Earth & Environment*, *1*, 284–299. https://doi.org/10.1038/s43017-020-0058-6

Hizzett, J. L., Hughes Clarke, J. E., Sumner, E. J., Cartigny, M. J. B., Talling, P. J., & Clare, M. A. (2018). Which triggers produce the most erosive, frequent, and longest runout turbidity currents on deltas? *Geophysical Research Letters*, *45*, 855–863. https://doi.org/10.1002/2017GL075751

Hood, E., Fellman, J. B., & Spencer, R. G. M. (2020). Glacier loss impacts riverine organic carbon transport to the ocean. *Geophysical Research Letters*, *47*(19), e2020GL089804. https://doi.org/10.1029/2020GL089804

Hoover, T. M., Marczak, L. B., Richardson, J. S., & Yonemitsu, N. (2010). Transport and settlement of organic matter in small streams. *Freshwater Biology*, *55*(2), 436–449. https://doi.org/10.1111/j.1365-2427.2009.02292.x

Hughes Clarke, J. E., Talling, P. J., & Cartigny, M. J. C. (2015). *Flow by flow monitoring within fjord-delta turbidite systems: Insights into deep water channel-to-lobe transitions*. Paper presented at American Geoscience Union Annual Meeting.

Hunter, W., Jamieson, A., Huvenne, V., & Witte, U. (2013). Sediment community responses to marine vs. terrigenous organic matter in a submarine canyon. *Biogeosciences*, *10*, 67–80. https://doi.org/10.5194/bg-10-67-2013

Kao, S.-J., Hilton, R. G., Selvaraj, K., Dai, M., Zehetner, F., Huang, J.-C., et al. (2014). Preservation of terrestrial organic carbon in marine sediments offshore Taiwan: Mountain building and atmospheric carbon dioxide sequestration. *Earth Surface Dynamics*, *2*, 127–139. https://doi.org/10.5194/esurf-2-127-2014

Lee, H., Galy, V., Feng, X., Ponton, C., Glay, A., France-Lanord, C., & Feakins, S. (2019). Sustained wood burial in the Bengal Fan over the last 29 million years. *Proceedings of the National Academy of Sciences of the United States of America*, *116*(45), 22518–22525. https://doi.org/10.1073/pnas.1913714116

Liu, J. T., Hsu, R. T., Hung, J.-J., Chang, Y.-P., Wang, Y.-H., Rendle-Bühring, R. H., & Yang, R. J. (2016). From the highest to the deepest: The Gaoping River–Gaoping Submarine Canyon dispersal system. *Earth-Science Reviews*, *153*, 274–300. https://doi.org/10.1016/j.earscirev.2015.10.012

MacDonald, R., MacDonald, D., O'Brien, M., & Gobeil, C. (1991). Accumulation of heavy metals (Pb, Zn, Cu, Cd), carbon and nitrogen in sediments from Strait of Georgia, BC, Canada. *Marine Chemistry*, *34*(1–2), 109–135. https://doi.org/10.1016/0304-4203(91)90017-q

McArthur, A., Kneller, B., Souza, P., & Kuchle, J. (2016). Characterization of deep-marine channel-levee complex architecture with palynofacies: An outcrop example from the Rosario Formation, Baja California, Mexico. *Marine and Petroleum Geology*, *73*, 157–173. https://doi.org/10.1016/j.marpetgeo.2016.02.030

McArthur, A. D., Kneller, B. C., Wakefield, M. I., Souza, P. A., & Kuchle, J. (2016). Palynofacies classification of the depositional elements of confined turbidite systems: Examples from the Gres d'Annot, SE France. *Marine and Petroleum Geology*, *77*, 1254–1273. https://doi.org/10.1016/j.marpetgeo.2016.08.020

Meidinger, D., & Pojar, J. (1991). Ecosystems of British Columbia. In D. Meidinger & J. Pojar (Eds.), *Special Report Series 6*. Victoria, BC: Research Branch BC Ministry of Forests. Retrieved from https://www.for.gov.bc.ca/hfd/pubs/docs/srs/srs06.htm

Pope, E. L., Cartigny, M. J. B., Clare, M. A., Talling, P. J., Lintern, D. G., Vellinga, A., et al. (2022). First source-to-sink monitoring shows dense head controls sediment flux and runout in turbidity currents. *Science Advance*, *8*, eabj3220. https://doi.org/10.1126/sciadv.abj3220

Pope, E. L., Normandeau, A., Ó Cofaigh, C., Stokes, C. R., & Talling, P. J. (2019). Controls on the formation of turbidity current channels associated with marine-terminating glaciers and ice sheets. *Marine Geology*, *415*. https://doi.org/10.1016/j.margeo.2019.05.010

Prior, D. B., Bornhold, B. D., & Johns, M. W. (1986). Active sand transport along a fjord-bottom channel, Bute Inlet, British Columbia. *Geology*, *14*(7), 581–584. https://doi.org/10.1130/0091-7613(1986)14<581:ASTAAF>2.0.CO;2

Prior, D. B., Bornholdt, B. D., Wiseman, W. J. J., & Lowe, D. R. (1987). Turbidity current activity in a British Columbia fjord. *Sciences, New Serie, American Association for the Advancement of Science*, *237*(4820), 1330–1333. https://doi.org/10.1126/science.237.4820.1330

Rabouille, C., Dennielou, B., Baudin, F., Raimonet, M., Droz, L., Khripounoff, A., et al. (2019). Carbon and silica megasink in deep-sea sediments of the Congo terminal lobes. *Quaternary Science Reviews*, *222*, 105854. https://doi.org/10.1016/j.quascirev.2019.07.036

Runkel, R. L., Crawford, C. G., & Cohn, T. A. (2004). *Load estimator (LOADEST): A FORTRAN program for estimating constituent loads in streams and rivers* (p. 69). U.S. Geological Survey Techniques and Methods.

Sadler, P. M. (1981). Sediment accumulation rates and the completeness of stratigraphic sections. *The Journal of Geology*, *89*(5), 569–584. https://doi.org/10.1086/628623

Smeaton, C., & Austin, W. E. N. (2019). Where's the carbon: Exploring the spatial heterogeneity of sedimentary carbon in mid-latitude fjords. *Frontiers of Earth Science*, *7*, 269. https://doi.org/10.3389/feart.2019.00269

Smith, R. W., Bianchi, T. S., Allison, M., Savage, C., & Galy, V. (2015). High rates of organic carbon burial in fjord sediments globally. *Nature Geoscience*, *8*, 450–453. https://doi.org/10.1038/ngeo2421

Soulet, G., Skinner, L., Beaupré, S. R., & Galy, V. (2016). A note on reporting of reservoir ^{14}C disequilibria and age offsets. *Radiocarbon*, *58*(1), 205–2011. https://doi.org/10.1017/rdc.2015.22

Syvitski, J. P. M., Asprey, K. W., Clattenburg, D. A., & Hodge, G. D. (1985). The prodelta environment of a fjord: Suspended particle dynamics. *Sedimentology*, *32*, 83–107. https://doi.org/10.1111/j.1365-3091.1985.tb00494.x

Syvitski, J. P. M., & Farrow, G. E. (1983). Structures and processes in Bayhead deltas: Knight and Bute Inlet, British Columbia. *Sedimentary Geology*, *36*(217), 244. https://doi.org/10.1016/0037-0738(83)90010-6

Syvitski, J. P. M., Smith, J. N., Calabrese, E. A., & Boudreau, B. P. (1988). Basin sedimentation and the growth of prograding deltas. *Journal of Geophysical Research*, *93*(C6), 6895–6908. https://doi.org/10.1029/JC093iC06p06895

Tabata, S., & Pickard, G. L. (1957). The physical oceanography of Bute Inlet, British Columbia. *Journal of the Fisheries Research Board of Canada*, *14*(4), 487–520. https://doi.org/10.1139/f57-014

Turowski, J. M., Hilton, R. G., & Sparker, R. (2016). Decadal carbon discharge by a mountain stream is dominated by coarse organic matter. *Geology*, *44*(1), 27–30. https://doi.org/10.1130/g37192.1

Underwood, G., Paterson, D., & Parkes, R. (1995). The measurement of microbial carbohydrate exopolymers from intertidal sediments. *Limnology & Oceanography*, *40*(7), 1243–1253. https://doi.org/10.4319/lo.1995.40.7.1243

Vanderkerkhove, E., Bertrand, S., Crescenzi Lanne, E., Reid, B., & Pantoja, S. (2020). Modern sedimentary processes at the heads of Martinez Channel and Steffen Fjord, Chilean Patagonia. *Marine Geology*, *419*, 106076.

Wang, T., Hamann, A., Spittlehouse, D., & Carroll, C. (2016). Locally downscaled and spatially customizable climate data for historical and future periods for North America. *PLoS One*, *11*(6), 1–17. https://doi.org/10.1371/journal.pone.0156720

Water Survey of Canada. (2020). *Historical hydrometric data*.

Waterson, E. J., & Canuel, E. A. (2008). Sources of sedimentary organic matter in the Mississippi River and adjacent Gulf of Mexico as revealed by lipid biomarker and δ^{13}C TOC analyses. *Organic Geochemistry*, *39*(4), 422–439. https://doi.org/10.1016/j.orggeochem.2008.01.011

West, A. J., Lin, C. W., Lin, T. C., Hilton, R. G., Liu, S. H., Chang, C. T., et al. (2011). Mobilization and transport of coarse woody debris to the oceans triggered by an extreme tropical storm. *Limnology & Oceanography*, *56*(1), 77–85. https://doi.org/10.4319/lo.2011.56.1.0077

Włodarska-Kowalczuk, M., Mazurkiewicz, M., Górska, B., Michel, L. N., Jankowska, E., & Zaborska, A. (2019). Organic carbon origin, benthic faunal consumption, and burial in sediments of northern Atlantic and Arctic fjords (60–81°N). *Journal of Geophysical Research: Biogeosciences*, *124*, 3737–3751.

Zeng, J., Lowe, D. R., Prior, D. B., Wiseman, W. J. J., & Bornhold, B. D. (1991). Flow properties of turbidity currents in Bute Inlet, British Columbia. *Sedimentology*, *38*(6), 975–996. https://doi.org/10.1111/j.1365-3091.1991.tb00367.x